

Stabilization of a Strained Heteroradialene by Peripheral Electron Delocalization

S. Hessam M. Mehr, Brian O. Patrick, and Mark J. MacLachlan

Department of Chemistry, University of British Columbia, 2036 Main Mall, Vancouver, BC
V6T 1Z1 CANADA

mmaclach@chem.ubc.ca

Materials	S2
Instrumentation	S2
X-ray Crystallography	S2
Cyclic Voltammetry	S2
NMR Spectroscopy	S3
Experimental	S3
NMR Spectra	S6
Ab initio calculations	S9
Geometry Optimization	S9
Conformational Analysis of Compound 3	S9
Calculation of Excited-State Energies	S10
Calculated Energy-Optimized Atomic Coordinates for 3 (S1)	S11
Calculated Energy-Optimized Atomic Coordinates for S2	S12
Calculated Energy-Optimized Atomic Coordinates for S3	S13
Calculated Energy-Optimized Atomic Coordinates for S4	S14
References	S15

Materials

All reagents and solvents were obtained from standard suppliers and used without purification. 1,3-Diformylphloroglucinol was prepared from phloroglucinol in 85% yield by following the literature procedure.¹ ¹⁵N-labelled dimethylamine hydrochloride was obtained from Berry & Associates.

Instrumentation

All reactions were carried out under air unless otherwise noted. High-resolution ESI mass spectra were obtained on a Waters/Micromass LCT time-of-flight (TOF) mass spectrometer. Infrared spectroscopy was carried out on a Thermo Scientific Nicolet 6700 (ATR) FT-IR instrument using the SmartOrbit attenuated total reflectance (ATR) accessory.

X-ray Crystallography

Slow evaporation of a 1:2 CH₂Cl₂–hexanes solution of compound **3** gave crystals suitable for single-crystal X-ray crystallography.

All measurements were made at a temperature of -183.0 ± 0.1 °C on a Bruker APEX DUO diffractometer using graphite monochromated Mo-K α (max $2\theta = 53.0^\circ$). Data was collected in a series of ϕ and ω scans in 0.5° oscillations using 15.0-second exposures. The crystal-to-detector distance was 38.21 mm. The material crystallizes as a two-component ‘split-crystal’ with components one and two related by a 180° rotation about the (0.00 0.00 1.00) reciprocal axis. Data were integrated for both components, including both overlapped and non-overlapped reflections. In total 13148 reflections were integrated (2245 from component one only, 2234 from component two only, 8669 overlapped). Data were collected and integrated using the Bruker SAINT software packages. Data were corrected for absorption effects using the multi-scan technique (TWINABS), with minimum and maximum transmission coefficients of 0.851 and 0.991, respectively. The data were corrected for Lorentz and polarization effects.

The structure was solved by direct methods² using non-overlapped data from the major twin component. Subsequent refinements were carried out using an HKLF 5 format data set containing complete data from component one and overlapped reflections from component two. All non-hydrogen atoms were refined anisotropically. All hydrogen atoms were placed in calculated positions. The final cycle of full-matrix least-squares refinement on F^2 was based on 2944 reflections and 197 variable parameters.

X-ray crystal data for **3**: C₁₅H₂₁N₃O₃, MW = 291.35 g mol⁻¹, colorless irregular crystal (0.10 × 0.17 × 0.28 mm³), triclinic, space group P-1 (#2), a = 6.433(2), b = 7.542(3), c = 15.771(6) Å, $\alpha = 90.874(6)^\circ$, $\beta = 95.675(7)^\circ$, $\gamma = 109.593(8)^\circ$, V = 716.5(4) Å³, Z = 2, $\rho_{\text{calcd}} = 1.351$ g cm⁻³, F₀₀₀ = 312.00, $\mu(\text{Mo-K}\alpha) = 0.95$ cm⁻¹, $\lambda(\text{Mo-K}\alpha) = 0.71073$ Å, GoF = 1.05; R1, wR2 = 0.065, 0.144 (all data); 0.052, 0.137 (F^2 : I > 2.00 σ (I)).

Cyclic Voltammetry

Cyclic voltammetry experiments were carried out on a Pine Instruments AFCBP1 potentiostat. The setup comprised dichloromethane as solvent, tetrabutylammonium hexafluorophosphate as electrolyte, a platinum mesh counter electrode, a glassy carbon working electrode, silver wire used as pseudoreference, and ferrocene (added after the measurement) as reference.

NMR Spectroscopy

All ^1H NMR and ^1H - ^{15}N HSQC spectra were measured on a 400 MHz Bruker spectrometer equipped with an inverse (proton detection) probe.

Direct observation of heteronuclei was accomplished on a 400 MHz Bruker spectrometer configured with a SmartProbeTM using a flip angle of 30° and inverse-gated (^{15}N) or power-gated (^{13}C) proton decoupling. To speed up longitudinal relaxation, about 4 mg of $\text{Cr}(\text{acac})_3$ was added. This relaxation agent was excluded in ^1H experiments to prevent signal broadening. The ^{15}N spectral reference was adjusted to the Bruker scale (liquid NH_3 at 0 ppm). A standard sample of 90% formamide in $\text{DMSO-}d_6$ was used as indirect reference to verify this.

For ^1H - ^{15}N HSQC a phase-sensitive pulse sequence incorporating gradient pulses and double INEPT transfer was used (HSQCETGP).^{3,4} A wide ^{15}N chemical shift window (250 ppm) was used initially and a 30 ppm area containing all ^{15}N - ^1H cross peaks was selected for subsequent measurements. Direct (see above) and indirect chemical shifts for ^{15}N agreed within the heteronuclear resolution of the HSQC experiment (24 Hz) in all cases.

All NMR experiments were carried out using Bruker TopSpinTM software and the data subsequently processed using ACD/Labs NMR Processor. For 1D heteronuclear spectra, an exponential window function with a line-broadening factor (LB) of 3.0 was employed.

Rotational activation barriers were calculated from the coalescence temperatures obtained in variable-temperature NMR experiments. The common definition⁵ of coalescence, $k_{\text{ex}} = \frac{\pi\Delta\nu}{\sqrt{2}}$ was used. The Eyring equation, $k_{\text{ex}} = \frac{k_{\text{B}}T}{h} e^{\frac{-\Delta G^\ddagger}{RT}}$ then yields

$$\Delta G^\ddagger = -RT_c \ln \frac{\pi h \Delta \nu}{\sqrt{2} k_{\text{B}} T_c}.$$

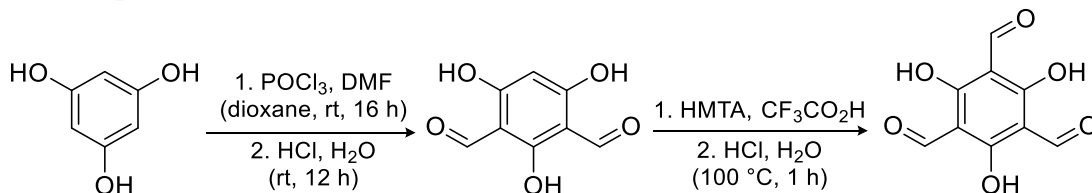
The uncertainty in ΔG^\ddagger was calculated based on an assumed T_c error of $\pm 5^\circ\text{C}$ and

$$\frac{\partial \Delta G^\ddagger}{\partial T_c} = \frac{\Delta G^\ddagger}{T_c} + R.$$

Experimental

The following improved procedure was used to prepare 2,4,6-triformylphloroglucinol **1** from 2,4-diformylphloroglucinol (DFP). DFP itself was prepared from phloroglucinol in 85% yield by following the literature procedure.¹

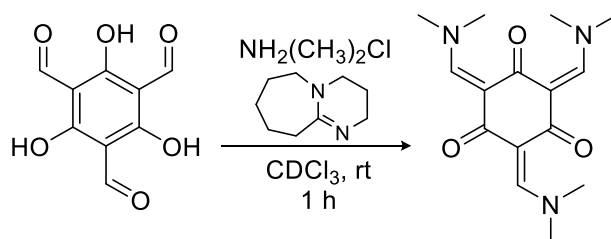
Scheme S1. Improved synthesis of **1**.



Synthesis of triformylphloroglucinol (1): Diformylphloroglucinol (6.00 g, 32.9 mmol, 1 equiv) and hexamethylenetetramine (6.96 g, 49.6 mmol, 1.5 equiv) were dried under high vacuum in a Schlenk flask at 60°C for 1.5 h. The flask was back-filled with N_2 and trifluoroacetic acid (38.0 mL, 496 mmol, 15 equiv) was added. Following 4 h of reacting at

100 °C under a nitrogen atmosphere, 2 M HCl (120 mL) was added and stirring continued under air at the same temperature for 1 h. During this period a large amount of orange precipitate formed, which was subsequently removed by filtration through celite. After cooling to room temperature, the supernatant was extracted with 3 × 50 mL of dichloromethane and the organic extract dried over anhydrous Na₂SO₄, filtered, and evaporated to give 4.12 g (19.6 mmol, 60%) of compound **1** as a salmon-orange powder. This is a substantial improvement on the previously reported syntheses of **1**.

Scheme S2. Synthesis of **3**

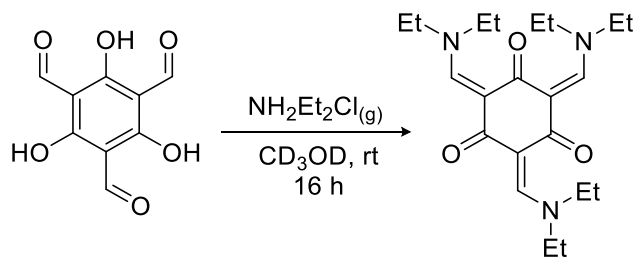


Synthesis of **3:** Triformylphloroglucinol **1** (10.0 mg, 0.0476 mmol, 1 equiv) was added to a septum-capped NMR tube containing 0.6 mL of CDCl₃ and dispersed by sonicating for 5 min. A septum-capped Schlenk flask was charged with 50 mg (0.61 mmol, 13 equiv) of anhydrous dimethylamine hydrochloride and 0.100 mL (101 mg, 0.67 mmol, 14 equiv) of 1,8-diazabicycloundec-7-ene (DBU) under nitrogen and sonicated until a viscous, white suspension was obtained. Dimethylamine was carried from the headspace of the Schlenk flask by nitrogen gas introduced through the sidearm and, using a steel cannula, bubbled into the NMR solvent. After 1 min, the Schlenk flask was brought in contact with a heating bath at 95 °C, causing bubbles of dimethylamine gas to form in the suspension. During the following 20 min, the suspension of **1** in CDCl₃ underwent a change of color from the initial pale yellow to a brilliant fluorescent yellow-green, to a bright orange.

At this point, the cannula was removed and the progress of the reaction was monitored by ¹H NMR spectroscopy. The reaction was complete after about 1 h, judging by the disappearance of the aldehyde peak. Evaporation of NMR solvent under high vacuum left 13.7 mg (0.0471 mmol, 99%) of an orange powder. ¹H NMR (400 MHz, CD₃OD) δ 8.10 (s, 3H; CH), 3.43 (s, 9H; CH₃), 3.19 (s, 9H; CH₃). ¹³C NMR (100 MHz, CDCl₃) δ 182.7 (CO, br), 159.5 (CH-N), 107.4 (C-CHN, br), 48.2 (CH₃), 44.4 (CH₃). ¹⁵N NMR (**3**-¹⁵N₃, 40 MHz, CD₃OD) δ 130.2. UV-Vis (CH₂Cl₂) λ_{max} (ε) = 363 (5.3 × 10⁴), 308 (4.1 × 10⁴), 257 (1.3 × 10⁴) nm (cm⁻¹ mol⁻¹ L). IR (neat) ν = 2918 (br), 2806, 1582, 1525, 1414, 1339, 1293, 1135, 1042, 998, 967, 944, 809, 733, 625, 588, 463 cm⁻¹. HRMS (ESI/TOF-Q) *m/z*: [**3** + H]⁺ Calcd for C₁₅H₂₂N₃O₃ 292.1661; Found 292.1663.

Synthesis of **3-¹⁵N₃:** The preparation of **3**-¹⁵N₃ was carried out identically to that of **3** except using ¹⁵N-labelled anhydrous dimethylamine hydrochloride instead of anhydrous dimethylamine hydrochloride. IR (neat) ν = 2917 (br), 2806, 1573, 1520, 1411, 1344, 1290, 1134, 1038, 997, 945, 810, 733, 624, 586, 461 cm⁻¹. HRMS (ESI/TOF-Q) *m/z*: [**3**-¹⁵N₃ + H]⁺ Calc'd for C₁₅H₂₂¹⁵N₃O₃ 295.1572; Found 295.1567 (base peak); Calcd for C₁₅H₂₂¹⁵N₂NO₃ 294.1602; Found 294.1581 (6.5%).

Scheme S3. Synthesis of **4**



Synthesis of 4: Triformylphloroglucinol **1** (10.0 mg, 0.0476 mmol, 1 equiv) was introduced to a septum-capped NMR tube containing 0.6 mL of CD_3OD ; the contents were degassed with N_2 . Diethylamine (0.10 mL, 71 mg, 0.97 mmol, 20 equiv) was injected into a Schlenk flask and the flask warmed up to 40°C to accelerate the evaporation of the amine while the gaseous diethylamine was bubbled into the NMR solvent through a canula. During the next 15 min the solids of **1** dissolved to give a yellow-orange solution. Following this, the canula was removed and the NMR tube stored at room temperature for 16 h. The ^1H NMR spectrum of the resulting orange-red solution shows virtually complete conversion of TFP to **4**, along with a large excess of diethylamine. Solvent and excess diethylamine were then removed at room temperature under high vacuum, leaving a dark crimson semi-solid. When dissolved in benzene, a light orange supernatant and small amounts of a sticky dark solid resulted. Evaporation of the supernatant under high vacuum gave a thick orange oil (17.7 mg, 0.0467 mmol, 98%) which is pure **4** by ^1H NMR spectroscopy. ^1H NMR (400 MHz, CDCl_3) δ 8.10 (s, 3H; CH), 3.88 (q, br, $^3J_{\text{HH}} = 7.04$ Hz, 6H; CH_2), 3.52 (q, br, $^3J_{\text{HH}} = 7.04$ Hz, 6H; CH_2), 1.33 (t, br, $^3J_{\text{HH}} = 7.04$ Hz, 9H; CH_3), 1.16 (t, br, $^3J_{\text{HH}} = 7.04$ Hz, 9H; CH_3). ^{13}C NMR (100 MHz, CDCl_3) δ 183.1 (CO), 157.2 (CH-N), 107.4 (C-CHN), 53.5 (CH_2), 47.8 (CH_2), 15.2 (CH_3), 12.7 (CH_3). UV-Vis (CH_2Cl_2) λ_{max} (ϵ) = 365 (3.6×10^4), 308 (3.5×10^4), 273 (3.0×10^4) nm ($\text{cm}^{-1} \text{mol}^{-1} \text{L}$). IR (**4**, neat) $\nu = 2926$ (br), 1591, 1508, 1414, 1371, 1138, 1043, 1003, 947, 810, 627, 590, 469 cm^{-1} . IR (neat glaze) $\nu = 2973$, 2934, 2873, 1573, 1515, 1442, 1389, 1346, 1301, 1259, 1178, 1138, 1049, 1020, 938, 924, 807, 619, 591, 529, 476 cm^{-1} . HRMS (ESI/TOF-Q) m/z : [**4** + H] $^+$ Calcd for $\text{C}_{21}\text{H}_{34}\text{N}_3\text{O}_3$ 376.2600; Found 376.2595.

NMR Spectra

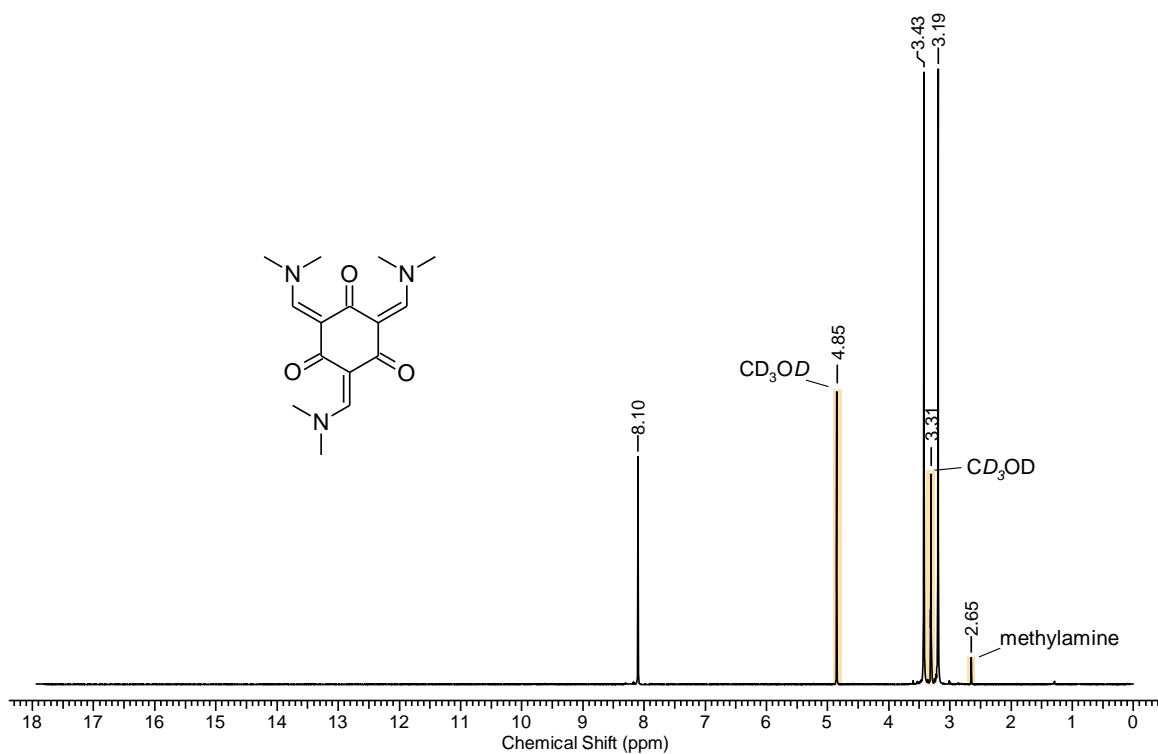


Figure S1. ^1H NMR spectrum of **3** (400 MHz, CD_3OD).

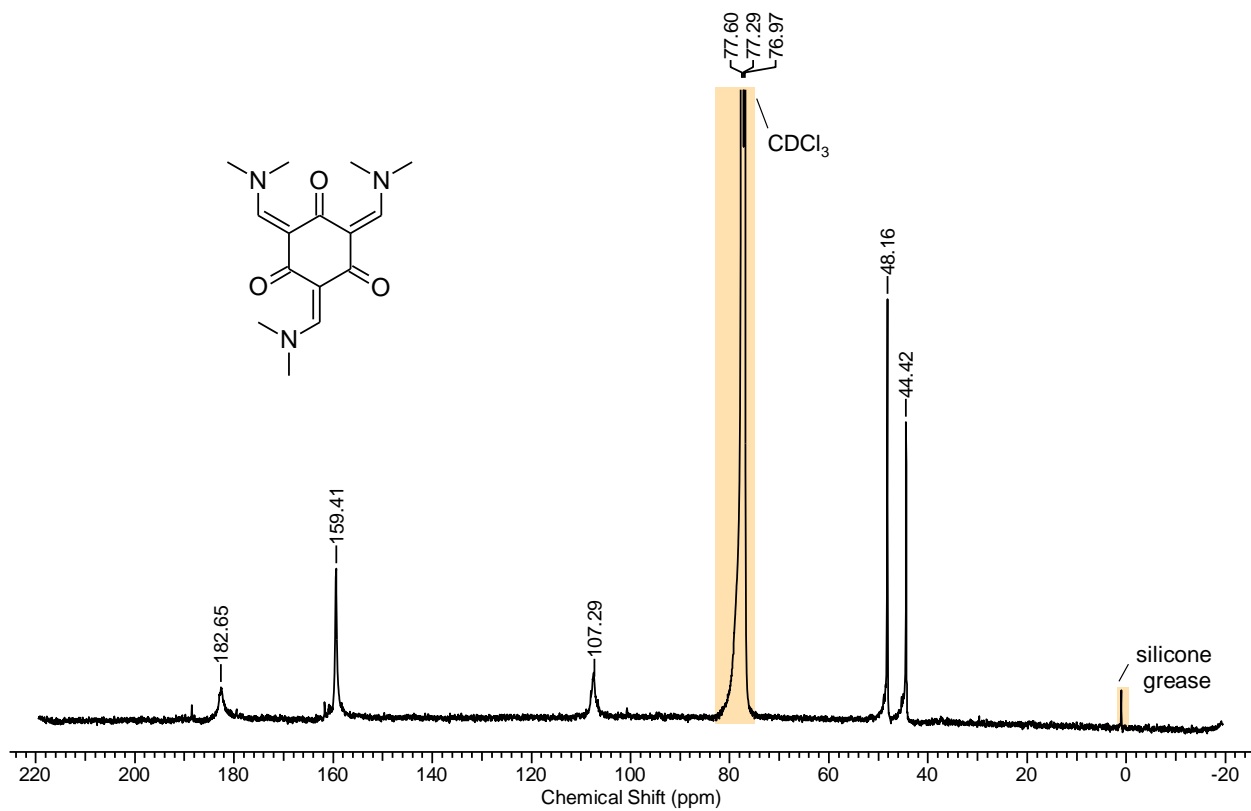


Figure S2. ^{13}C NMR spectrum of **3** (100 MHz, CDCl_3).

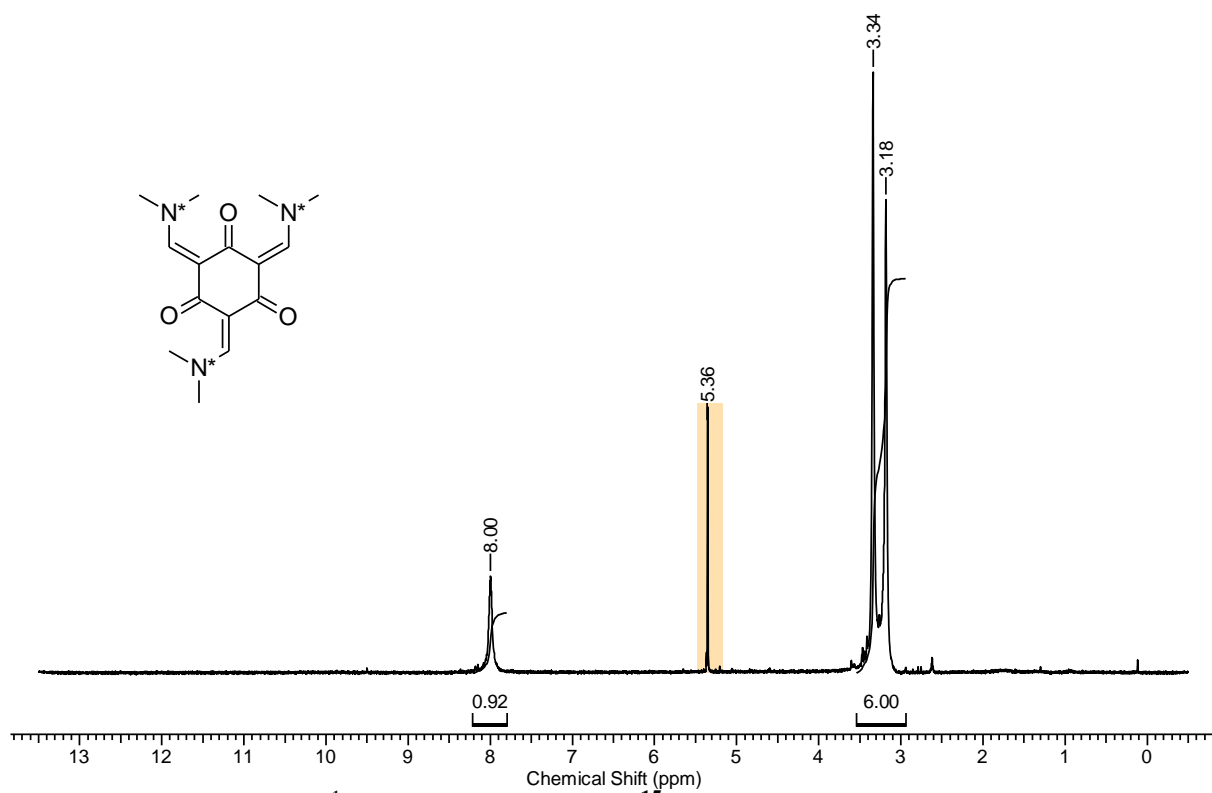


Figure S3. ¹H NMR spectrum of 3-¹⁵N₃ (400 MHz, CD₂Cl₂).

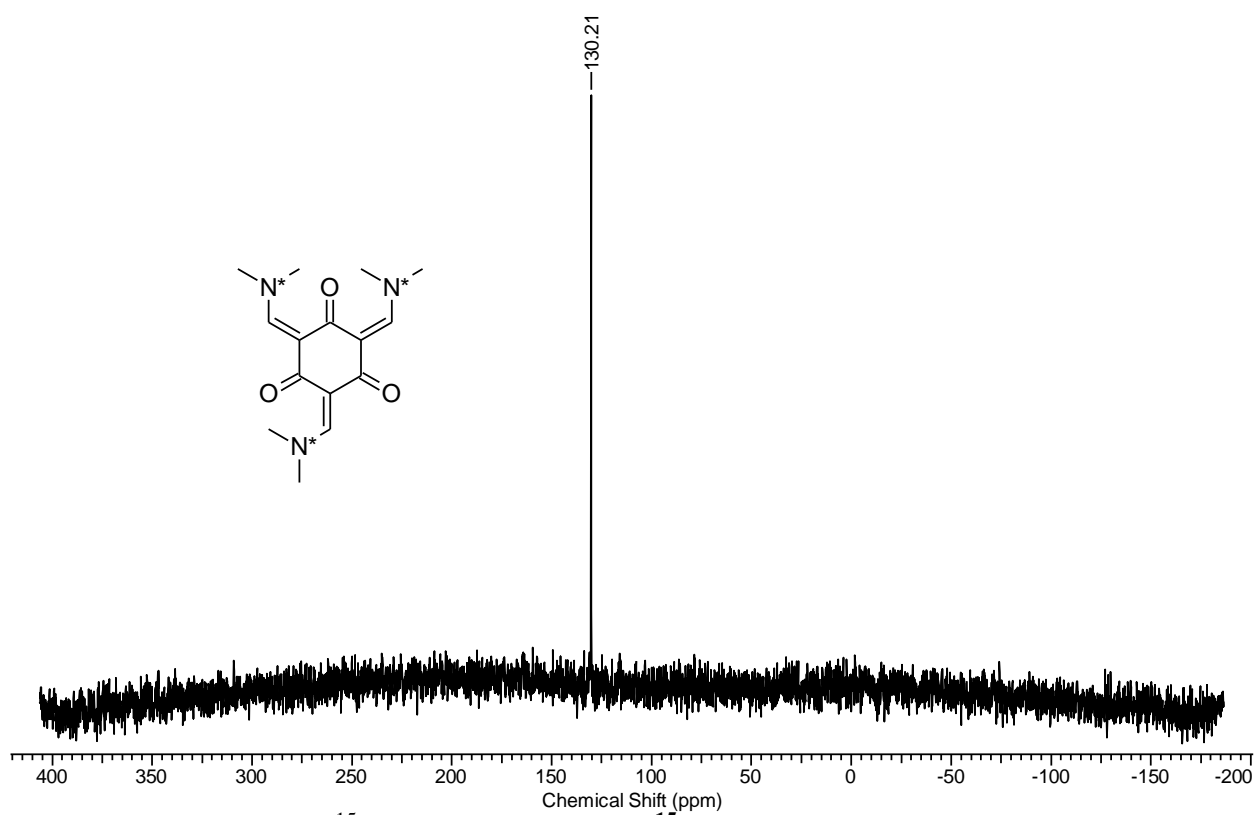


Figure S4. ¹⁵N NMR spectrum of 3-¹⁵N₃ (40 MHz, CD₃OD).

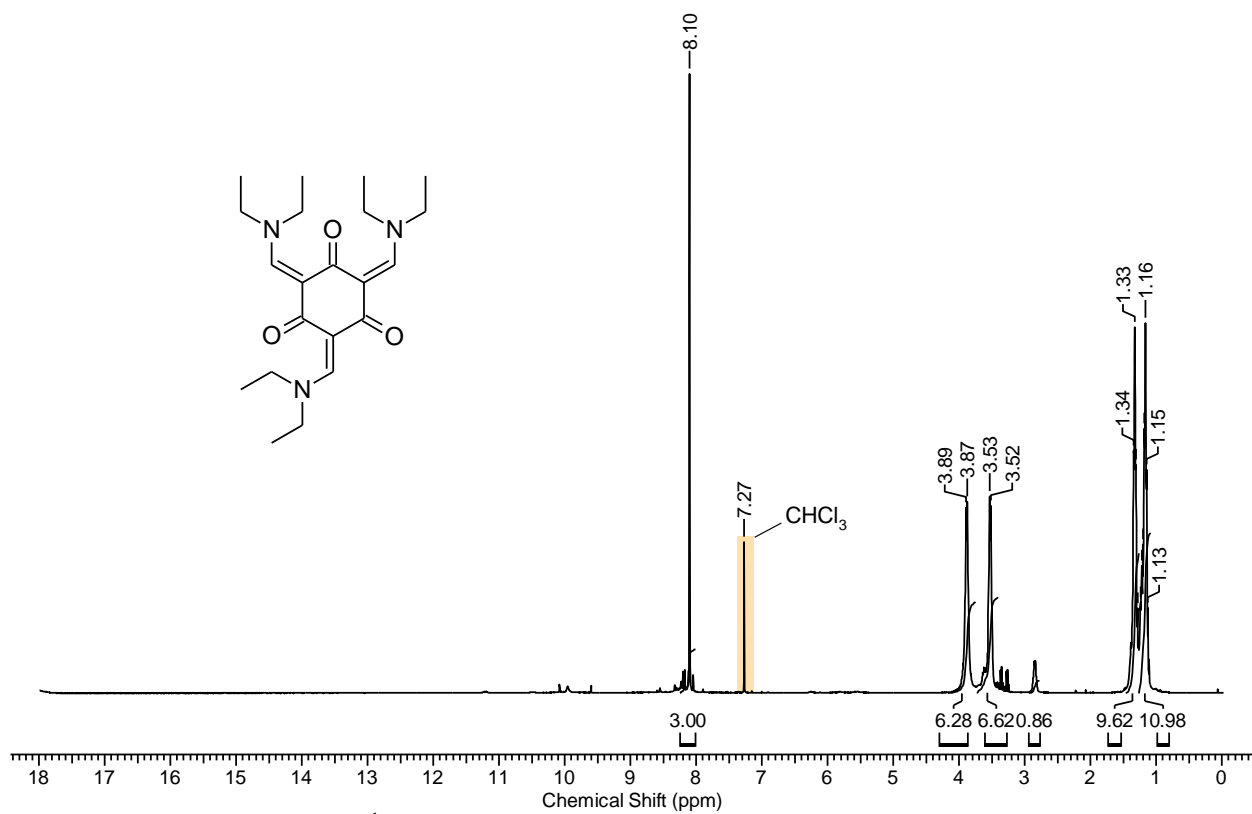


Figure S5. ^1H NMR spectrum of **4** (400 MHz, CDCl_3).

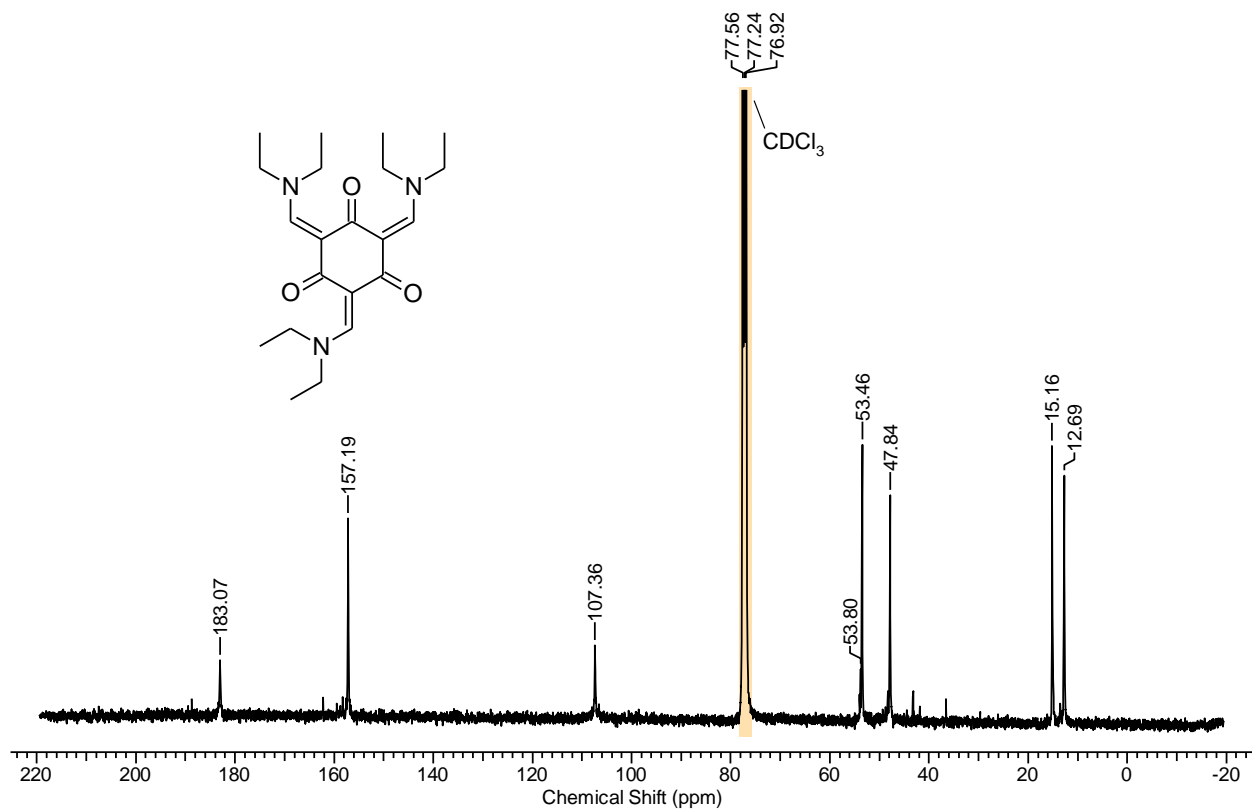


Figure S6. ^{13}C NMR spectrum of **4** (100 MHz, CDCl_3).

Ab initio calculations

All ab initio calculations were carried out using Gaussian 09⁶. Specifically, density functional theory (DFT) was used with the Minnesota 06⁷ (M06) functional and a Dunning-type triple zeta correlation consistent basis set (cc-pVTZ)⁸⁻¹⁰. In all cases, the polarizable continuum model (PCM)¹¹ was used to model the effects of bulk solvent. For geometry optimizations, the final structure was checked for the absence of imaginary frequencies.

Geometry Optimization

The atomic coordinates obtained from single-crystal X-ray diffraction of **3** were subjected to energy optimization in bulk CH₂Cl₂. Figure S7 shows the initial and final geometry along with the evolution of the O¹C¹¹C¹²C¹⁵ and O³C¹⁸C¹⁰C¹⁵ dihedral angles. The former is relaxed by less than 2° while the latter's deviation from planarity becomes more pronounced.

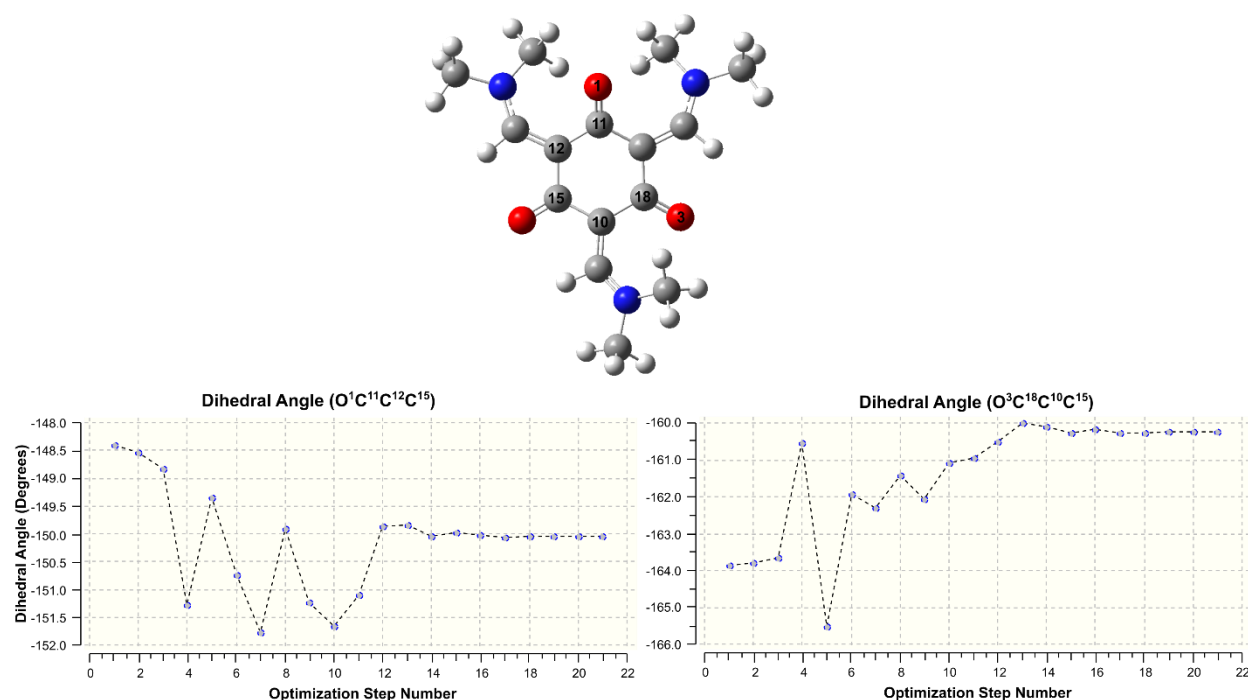


Figure S7: Energy optimized geometry for **3** (top) and the evolution of the O¹C¹¹C¹²C¹⁵ (bottom left) and O³C¹⁸C¹⁰C¹⁵ (bottom right) dihedral angles.

Conformational Analysis of Compound **3**

NMR experiments at low temperature revealed an asymmetric conformer of **3** as the majority species. Does the conformation in this maximally stable conformer resemble that seen in the solid state? To answer this question, we manually constructed and optimized the geometry of a number of alternative conformations of **3** with different orientations of the =CH-N(CH₃)₂ arms.

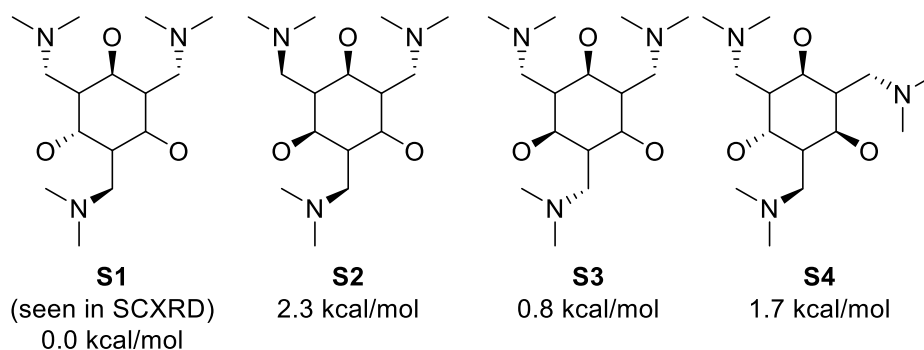


Figure S8. Relative energy values for optimized candidate geometries of 3 relative to S1.

As Figure S8 shows, starting with the geometry seen in the solid state leads to the lowest-energy isomer (**S1**) among the examined candidates. However, given the small energy difference and the limitations of the PCM model, one can only speculate that **S1** is the dominant structure seen in our low-temperature NMR experiments.

Calculation of Excited-State Energies

Time-dependent density functional theory^{12–15} was used to search for the lowest-lying singlet excited states. Table S1 summarizes the results the transitions with oscillator strength > 0.1. For each excitation, the contribution of each major Slater determinant is presented as $100\% \times 2x^2$ where x is the coefficient for the determinant in the configuration interaction (CI) expansion in the Gaussian output.

Table S1. Electronic excited states of 3.

Energy (eV)	Wavelength (nm)	Oscillator strength	Contributors		
			from	to	%
3.5462	349.63	0.1410	HOMO	LUMO	79
			HOMO-2	LUMO	17
			HOMO-5	LUMO+2	2
			HOMO-4	LUMO+1	4
3.7774	328.23	0.1169	HOMO-2	LUMO	66
			HOMO-1	LUMO	6
			HOMO	LUMO	18
3.8124	325.21	0.4751	HOMO-2	LUMO	4
			HOMO-1	LUMO	92
			HOMO-5	LUMO	3
4.3405	285.64	0.4001	HOMO-3	LUMO	10
			HOMO-1	LUMO+1	36
			HOMO-1	LUMO+2	8
			HOMO	LUMO+2	37
4.4028	281.60	0.3076	HOMO-3	LUMO	9
			HOMO-1	LUMO+1	22
			HOMO-1	LUMO+2	53

4.4218	280.39	0.1440	HOMO	LUMO+1	11
			HOMO-3	LUMO	57
			HOMO-1	LUMO+1	11
			HOMO-1	LUMO+2	21
			HOMO	LUMO+2	5

Calculated Energy-Optimized Atomic Coordinates for 3 (S1)

The atomic coordinates for **3** obtained from single-crystal X-ray diffraction were subjected to energy optimization in bulk (PCM) CH₂Cl₂. The following listing shows the Cartesian coordinates of the optimized structure in angstroms.

O	-2.08466700	0.38131600	1.08307700
O	0.95641700	-2.82736700	-0.32154800
O	2.08469700	1.68526300	-0.55621700
N	-2.96712900	-2.33380300	0.00617900
N	4.10219600	-0.46000700	0.07383900
N	-1.56527800	3.16363900	-0.09695100
C	-0.14151200	1.15603000	0.00488200
C	-1.64560300	-2.30776800	0.09437100
H	-1.18680000	-3.29142400	0.16098400
C	1.64819900	-0.58223900	-0.12294900
C	-1.08968800	0.12065500	0.40021600
C	-0.75696300	-1.25350800	0.03965500
C	-0.41649900	2.50658500	-0.00874800
H	0.45930800	3.15072600	-0.00512200
C	0.63907300	-1.64257000	-0.16122200
C	2.95119300	-1.03701900	-0.22472100
H	3.04841300	-2.06890700	-0.55414600
C	1.26686600	0.81829600	-0.22818400
C	-2.82086600	2.55459400	-0.47929500
H	-2.62789200	1.72181300	-1.15467900
H	-3.41702500	3.30313500	-1.00039700
H	-3.37091100	2.17134000	0.37903000
C	-3.68915400	-3.56605100	0.25436100
H	-2.99161000	-4.36096100	0.50441600
H	-4.26398200	-3.85371000	-0.62781300
H	-4.38305800	-3.43804100	1.08708200
C	-3.77527800	-1.21669300	-0.43264100
H	-4.08723100	-0.58453300	0.39761800
H	-4.65003600	-1.61225300	-0.94818600
H	-3.20098700	-0.60313900	-1.12558100
C	4.23972800	0.74175600	0.87109400
H	4.34990700	1.63109200	0.25389800
H	5.11977800	0.62278100	1.50421200
H	3.36165400	0.86884900	1.49820800

C	-1.59574000	4.60164900	0.07982900
H	-2.23435200	4.86846500	0.92398900
H	-1.99178300	5.08584700	-0.81477200
H	-0.59317600	4.97365800	0.27454800
C	5.35110700	-1.10681800	-0.27973400
H	5.93228200	-1.32620400	0.61781300
H	5.94508000	-0.45203600	-0.91956200
H	5.15312700	-2.03038800	-0.81699900

Calculated Energy-Optimized Atomic Coordinates for S2

O	2.35895800	0.68476800	0.19308800
O	-0.64663900	-2.89716000	0.39656600
O	-2.11920600	1.29189500	-1.02013700
N	3.19332500	-2.16627500	-0.12748900
N	-3.98598400	-0.80857700	0.09753900
N	1.04323500	3.40609600	0.14915400
C	0.07732100	1.14407600	-0.15410400
C	1.91578200	-2.14828000	0.21362900
H	1.56351800	-3.08754600	0.63470600
C	-1.52535300	-0.76031900	-0.04692200
C	1.20894400	0.25250700	0.06013100
C	0.93600600	-1.17930500	0.07866100
C	0.17559700	2.51389200	-0.30494800
H	-0.64223500	2.95427400	-0.87172300
C	-0.42771900	-1.69947100	0.17380400
C	-2.78203400	-1.33888900	-0.03749900
H	-2.78339000	-2.42490500	-0.09282700
C	-1.25891300	0.61025100	-0.45349700
C	1.97421600	3.19205300	1.23856800
H	1.68925200	2.31270700	1.80488900
H	1.93593900	4.07164800	1.88485400
H	2.99395700	3.05733400	0.88143500
C	4.04128000	-3.26091900	0.30326800
H	3.48115200	-3.93687200	0.94363800
H	4.89397500	-2.87524100	0.86480500
H	4.42152400	-3.80950600	-0.56055400
C	3.81996100	-1.24521800	-1.05445800
H	4.48560300	-1.82448200	-1.69720700
H	4.39283800	-0.47613100	-0.53996800
H	3.06385100	-0.75941300	-1.66258600
C	-4.24051900	0.54015300	0.55843300
H	-5.16045900	0.52746700	1.14323800
H	-4.33577200	1.24300800	-0.26706000
H	-3.41975000	0.87080200	1.19102300
C	0.98622900	4.77352400	-0.32904700
H	1.94840200	5.06120600	-0.75703800

H	0.76229700	5.45608700	0.49348300
H	0.22374300	4.87114700	-1.09715000
C	-5.16599200	-1.62511700	-0.11026900
H	-5.76974800	-1.21551600	-0.92198300
H	-5.77728300	-1.64555800	0.79361000
H	-4.87519800	-2.63886000	-0.37264900

Calculated Energy-Optimized Atomic Coordinates for S3

O	-2.28229000	0.41776700	0.86819900
O	0.95282300	-2.84225200	0.26820100
O	2.13562400	1.67570800	0.50992500
N	-2.95783800	-2.33707600	-0.19505900
N	4.06865000	-0.49057500	-0.25115700
N	-1.50199800	3.19625800	-0.04185700
C	-0.14914800	1.16023500	0.23825000
C	-1.67569500	-2.30363000	0.13718800
H	-1.24496300	-3.28115900	0.33898400
C	1.63369100	-0.59010600	0.15947100
C	-1.16888600	0.13440200	0.41200700
C	-0.78294900	-1.25279900	0.18926000
C	-0.40857000	2.51415600	0.26862400
H	0.44434500	3.13767800	0.52508700
C	0.62599600	-1.65050200	0.22233000
C	2.93858700	-1.05597400	0.13466700
H	3.05221500	-2.09426400	0.43725000
C	1.27741900	0.81264300	0.29426200
C	-2.63909600	2.63617300	-0.74008800
H	-2.30323400	1.83651400	-1.39988800
H	-3.09132900	3.42535800	-1.34022400
H	-3.37605900	2.21834400	-0.05601000
C	-3.71920200	-3.55941300	-0.02795800
H	-3.08752800	-4.33435500	0.39823200
H	-4.11002500	-3.89964200	-0.98874600
H	-4.56252900	-3.39084700	0.64398100
C	-3.65791100	-1.25129000	-0.84798000
H	-4.10230200	-0.55987900	-0.13359000
H	-4.43094200	-1.68069800	-1.48468100
H	-2.95964900	-0.68897600	-1.46721900
C	4.16229400	0.71454200	-1.04970500
H	4.98862700	0.58587500	-1.75001300
H	4.33499500	1.59738800	-0.43784600
H	3.24136100	0.85827200	-1.60731800
C	-1.56145400	4.62375700	0.20214200
H	-2.38108200	4.85860700	0.88363300
H	-1.72880900	5.16243100	-0.73250500
H	-0.63154900	4.96318700	0.65084400

C	5.33313500	-1.15515300	0.00120100
H	5.97798900	-0.51655400	0.60742000
H	5.84555600	-1.36366100	-0.93965100
H	5.16469200	-2.08591100	0.53614700

Calculated Energy-Optimized Atomic Coordinates for S4

O	-2.13960602	-1.51538219	0.64586297
O	-0.29222219	2.71353012	-0.10720392
O	2.20766236	-1.08355250	-1.03859579
N	-3.78981730	0.88806454	-0.10465950
N	2.70910186	2.72649623	0.05625173
N	1.14782424	-3.65002885	0.19543529
C	0.11637639	-1.41533357	-0.01816683
C	-2.54589901	1.28559119	0.11134125
H	-2.45884601	2.34653117	0.33350657
C	1.13163279	0.84953042	-0.20394958
C	-1.20038532	-0.82436910	0.23468675
C	-1.34203582	0.61009062	0.03993308
C	0.14539730	-2.79423713	0.06916535
H	-0.83436147	-3.26596887	0.09031803
C	-0.16679817	1.48463190	-0.04768896
C	2.31632406	1.53851526	-0.37597494
H	3.08581331	0.99082193	-0.91531872
C	1.22855268	-0.59323739	-0.46855828
C	2.49800395	-3.29009604	0.57473999
H	2.48668234	-2.36922837	1.15219023
H	3.14043550	-3.14119083	-0.29122841
H	2.89661435	-4.09430403	1.19387060
C	-4.89700022	1.76536860	0.22096157
H	-4.52464272	2.68927700	0.65566183
H	-5.55975171	1.28392732	0.94226228
H	-5.47700453	1.99427946	-0.67512622
C	-4.16016927	-0.33778130	-0.78170680
H	-5.03038417	-0.12479294	-1.40408700
H	-4.39743525	-1.13583185	-0.08070057
H	-3.34130869	-0.67255745	-1.41264979
C	2.04668134	3.48680721	1.09691903
H	1.37793173	4.24229471	0.68975473
H	2.81760525	3.96618646	1.70204149
H	1.46158347	2.81981900	1.72460293
C	0.90441285	-5.07360197	0.06690131
H	1.18069715	-5.59102942	0.98748509
H	1.50078550	-5.48644071	-0.74881744
H	-0.14584932	-5.25386752	-0.14679379
C	3.96891508	3.28163968	-0.39803559
H	4.65191637	3.41514628	0.44316564

H	3.80469810	4.25583343	-0.86190757
H	4.42433418	2.62149795	-1.13133270

References

- (1) Lawrence, A. L.; Adlington, R. M.; Baldwin, J. E.; Lee, V.; Kershaw, J. A.; Thompson, A. L. *Org. Lett.* **2010**, *12*, 1676.
- (2) Sheldrick, G. M. *Acta Crystallogr. Sect. A Found. Adv.* **2015**, *71*, 3.
- (3) Bax, A.; Ikura, M.; Kay, L. E.; Torchia, D. A.; Tschudin, R. *J. Magn. Reson.* **1990**, *86*, 304.
- (4) Norwood, T. J.; Boyd, J.; Heritage, J. E.; Soffe, N.; Campbell, I. D. *J. Magn. Reson.* **1990**, *87*, 488.
- (5) Levitt, M. H. *Spin Dynamics: Basics of Nuclear Magnetic Resonance*, 2nd ed.; John Wiley & Sons, 2008.
- (6) Frisch, M. J.; Trucks, G. W.; Schlegel, H. B.; Scuseria, G. E.; Robb, M. A.; Cheeseman, J. R.; Scalmani, G.; Barone, V.; Mennucci, B.; Petersson, G. A.; Nakatsuji, H.; Caricato, M.; Li, X.; Hratchian, H. P.; Izmaylov, A. F.; Bloino, J.; Zheng, G.; Sonnenberg, J. L.; Hada, M.; Ehara, M.; Toyota, K.; Fukuda, R.; Hasegawa, J.; Ishida, M.; Nakajima, T.; Honda, Y.; Kitao, O.; Nakai, H.; Vreven, T.; Montgomery Jr., J. A.; Peralta, J. E.; Ogliaro, F.; Bearpark, M.; Heyd, J. J.; Brothers, E.; Kudin, K. N.; Staroverov, V. N.; Kobayashi, R.; Normand, J.; Raghavachari, K.; Rendell, A.; Burant, J. C.; Iyengar, S. S.; Tomasi, J.; Cossi, M.; Rega, N.; Millam, J. M.; Klene, M.; Knox, J. E.; Cross, J. B.; Bakken, V.; Adamo, C.; Jaramillo, J.; Gomperts, R.; Stratmann, R. E.; Yazyev, O.; Austin, A. J.; Cammi, R.; Pomelli, C.; Ochterski, J. W.; Martin, R. L.; Morokuma, K.; Zakrzewski, V. G.; Voth, G. A.; Salvador, P.; Dannenberg, J. J.; Dapprich, S.; Daniels, A. D.; Farkas, Ö.; Foresman, J. B.; Ortiz, J. V.; Cioslowski, J.; Fox, D. J. Gaussian Inc.: Wallingford, CT 2009,.
- (7) Zhao, Y.; Truhlar, D. G. *Theor. Chem. Acc.* **2008**, *120*, 215.
- (8) Dunning, T. H. *J. Chem. Phys.* **1989**, *90*, 1007.
- (9) Kendall, R. A.; Dunning, T. H.; Harrison, R. J. *J. Chem. Phys.* **1992**, *96*, 6796.
- (10) Davidson, E. R. *Chem. Phys. Lett.* **1996**, *260*, 514.
- (11) Tomasi, J.; Mennucci, B.; Cammi, R. *Chem. Rev.* **2005**, *105*, 2999.
- (12) Bauernschmitt, R.; Ahlrichs, R. *Chem. Phys. Lett.* **1996**, *256*, 454.
- (13) Casida, M. E.; Jamorski, C.; Casida, K. C.; Salahub, D. R. *J. Chem. Phys.* **1998**, *108*, 4439.

- (14) Stratmann, R. E.; Scuseria, G. E.; Frisch, M. J. *J. Chem. Phys.* **1998**, *109*, 8218.
- (15) Furche, F.; Ahlrichs, R. *J. Chem. Phys.* **2002**, *117*, 7433.